Supplement of Atmos. Chem. Phys., 17, 11273–11292, 2017
https://doi.org/10.5194/acp-17-11273-2017-supplement


Atmospheric Chemistry and Physics
Open Access
EGU

*Supplement of*

# Higher measured than modeled ozone production at increased $NO_x$ levels in the Colorado Front Range

**Bianca C. Baier et al.**

*Correspondence to:* Bianca C. Baier (bianca.baier@noaa.gov)

# 1 MOPS raw $P(O_3)$ correction

In prior work, it was found that the MOPS technique can produce both positive and negative $O_3$ production rates that appear to be roughly correlated with temperature, relative humidity, or actinic flux (Baier et al., 2015). These artificial signals were also evident in first-generation MOPS (Cazorla et al., 2012). As described in the main text, we quantify the MOPS diurnal $O_3$ analyzer drift through zeroing techniques to provide a correction to the raw $P(O_3)$ data. This "zeroing" of the MOPS chambers involves removing the reference chamber film for an entire day (such that the net $P(O_3)$ in both chambers is equal), or by measuring $P(O_3)$ on cooler, cloudy days when $O_3$ formation is near zero. Diurnal $P(O_3)$ signals are then subtracted from the raw $P(O_3)$ signal to derive a corrected $P(O_3)$.

To track diurnal ozone analyzer drifting, four zeros were applied to the raw $P(O_3)$ data during this study for an entire 24-hour period with two using low ozone production days as zeros. However, previous studies have found that commercial $O_3$ analyzers can exhibit both positive and negative responses to changes in relative humidity due to increases or decreases in water vapor (US EPA, 1999; Wilson and Birks, 2006). Thus, the MOPS Thermo Scientific $O_3$ analyzer can possibly exhibit exaggerated drifting due to relative humidity changes. We have since conducted additional laboratory testing to investigate the relative humidity sensitivity of the Thermo Scientific $O_3$ analyzer used in this Golden, CO study. Although we note that artificial positive and negative $P(O_3)$ can be correlated with temperature, differences in temperature between sample and reference chamber did not play a large role in initiating baseline drifting. However, the MOPS $O_3$ analyzer did exhibit large baseline shifts greater than 2 ppbv when air enters the analyzer at relative humidities greater than 70%. Due to this relative humidity dependent baseline drifting, the MOPS raw $P(O_3)$ data correction techniques are adjusted from Baier et al. (2015) so as to minimize MOPS measurement days when $O_3$ analyzer drifting was more severe. Because the MOPS ozone analyzer is sheltered in an environment that is air conditioned to temperatures below ambient values, the MOPS ozone analyzer relative humidity does exceed 70% based on laboratory calculations using an expected MOPS analyzer environment temperature and the ambient vapor pressure. Thus, MOPS data are filtered to times when the air entering the ozone analyzer has a relative humidity below 70%. Furthermore, zeros that were taken only on days with diurnal patterns and absolute values of relative humidity

within the range of relative humidities measured on non-zeroing, MOPS measurements days were used to correct the raw $P(O_3)$ data. These time periods should capture the average $P(O_3)$ baseline drift throughout the campaign. Due to this zero filtering, one zero was discarded leaving three to be used to correct the raw $P(O_3)$ data. The average zero correction that is subtracted from the raw $P(O_3)$ measurements in order to derive the corrected $P(O_3)$ is shown in Fig. S1.

We have further tested the robustness of this threshold using a wide range of analyzer relative humidities to ensure that our corrected $P(O_3)$ values were not sensitive to this threshold choice. This testing was done by varying the temperature of the MOPS ozone analyzer to replicate field conditions. Figure S2 shows the half-hourly median MOPS $P(O_3)$ diurnal signal that results from varying the analyzer relative humidity. As seen in Fig. S2, the average 30-minute $P(O_3)$ patterns throughout the day are robust, with all corrected $P(O_3)$ scenarios peaking at approximately 1000 LT between 8-15 ppbv $h^{-1}$ regardless of the relative humidity threshold choice.

## 2 Aircraft VOC measurements

Constant, median mixing ratios of VOCs measured on the NCAR C-130 and NASA P-3B during the FRAPPÈ and DISCOVER-AQ field campaigns are used to supplement whole-air canister VOCs and further constrain the RACM2 and MCMv331 chemical models used in this study. Median mixing ratios and standard deviations of species for MOPS measurement days are shown in Table S1. Mixing ratios are calculated for only measurement points less than 1 km asl for the vicinity of Golden, CO, and a well-mixed boundary layer is assumed.

## 3 Model uncertainty analyses

To calculate the RACM2 uncertainty, we use a Random Sampling-High Dimensional Model Representation (RS-HDMR) technique outlined in Chen et al. (2012) and Chen and Brune (2012). Median values of all model inputs are calculated for the following two-hour time periods: 0600-0800 LT, 0800-1000 LT, 1000-1200 LT, 1200-1400 LT, and 1400-1800 LT. In total, 7 inorganic species, 32 VOC groups, 34 photolysis rates, 443 reaction rate coefficients, 615 product yields, and 168 deposition rates were randomly varied across their respective uncertainty ranges to determine the influence of input perturbations on model $P(O_3)$. Input uncertainties are outlined in Table S2.

To further reduce computational time, the Morris Method is used to pre-screen model constraints, identifying roughly 50-100 of the most influential inputs on the model output, $P(O_3)$ (Morris, 1991). The $P(O_3)$ variation due to changes in influential inputs and parameters is computed using Aerodyne Research, Inc. ExploreHD software (http://www.aerodyne.com/products/explorehd), decomposing the contribution of individual model inputs on the $P(O_3)$ output. The RACM2 RS-HDMR model $P(O_3)$ uncertainties are determined as the standard deviation in calculated $P(O_3)$ divided by its mean $P(O_3)$ for each time period above (Table S4).

The MCMv331 uncertainty is calculated for the same time periods between 0600-1800 LT by perturbing model constraints one-at-a-time to both their upper or lower uncertainty limits in a local sensitivity analysis. That is, for each sensitivity run, each variable or group of variables is adjusted to its upper or lower uncertainty values while keeping all other constraints at their original values. The following input groups are perturbed one at a time to examine its effect on MCMv331-calculated $P(O_3)$: $NO_x$ ($NO_2$ + NO), $O_3$, photolysis rates (J-values), all measured VOCs, product yields, and reaction rate coefficients. We select and vary reaction rate coefficients and product yields that are considered to be influential from the RACM2 RS-HDMR analysis. The MCMv331 input and parameter uncertainties ($1\sigma$) for these selected parameters are shown in Table S3.

The percent differences for each sensitivity run from the MCMv331 base run are shown in Fig. S3. All upper and lower percent deviations in Fig. S3 are added in quadrature to determine total upper and lower uncertainty bounds for MCMv331 $P(O_3)$. Hourly uncertainties for MCMv331 $P(O_3)$ are averaged for each RACM2 uncertainty time period and shown in Table S4.

# 4 $NO_x$-VOC sensitivity

Several metrics are used to assess $NO_x$-VOC sensitivity. In this study, we calculate the metric $L_N/Q$ in RACM2, which represents the fraction of free radicals removed by $NO_x$ (Kleinman et al., 2001). A $L_N/Q$ value greater than 0.5 represents a VOC-sensitive regime whereas a $L_N/Q$ value less than 0.5 represents a $NO_x$-sensitive regime. This metric was calculated for full-campaign data on MOPS measurement days and suggests that before 1200 LT, ozone production is VOC-sensitive where decreases in VOCs will be more effective in decreasing $P(O_3)$ and subsequent $NO_x$ decreases will act to increase $P(O_3)$ (Fig. S4). After 1200 LT, $P(O_3)$ is primarily $NO_x$ sensitive, where

decreasing $NO_x$ will linearly decrease $P(O_3)$. Higher measured $P(O_3)$ and $HO_2$ at higher $NO_x$ would suggest that there is a longer time period in the morning where $P(O_3)$ is $NO_x$-sensitive.

# References


Atkinson, R., 1991: Kinetics and Mechanisms of the Gas-Phase Reactions of the NO3 Radical with Organic Compounds. *Journal of Physical and Chemical Reference Data*, **20 (3)**, 459–507, doi:10.1063/1.555887, URL http://scitation.aip.org/content/aip/journal/jpcrd/20/3/10.1063/1.555887.

Atkinson, R., and S. M. Aschmann, 1989: Rate constants for the gas-phase reactions of the OH radical with a series of aromatic hydrocarbons at 296 ± 2 K. *Int. J. Chem. Kinet.*, **21 (5)**, 355–365, doi:10.1002/kin.550210506, URL http://onlinelibrary.wiley.com/doi/10.1002/kin.550210506/abstract.

Atkinson, R., and Coauthors, 2006: Evaluated kinetic and photochemical data for atmospheric chemistry Volume II: gas phase reactions of organic species. *Atmos. Chem. Phys.*, **6 (11)**, 3625–4055, doi:10.5194/acp-6-3625-2006, URL http://www.atmos-chem-phys.net/6/3625/2006/.

Baier, B. C., W. H. Brune, B. L. Lefer, D. O. Miller, and D. K. Martins, 2015: Direct ozone production rate measurements and their use in assessing ozone source and receptor regions for Houston in 2013. *Atmospheric Environment*, **114**, 83–91, doi:10.1016/j.atmosenv.2015.05.033, URL http://www.sciencedirect.com/science/article/pii/S1352231015301060.

Cazorla, M., W. H. Brune, X. Ren, and B. Lefer, 2012: Direct measurement of ozone production rates in Houston in 2009 and comparison with two estimation methods. *Atmos. Chem. Phys.*, **12 (2)**, 1203–1212, doi:10.5194/acp-12-1203-2012.

Chen, S., and W. H. Brune, 2012: Global sensitivity analysis of ozone production and O3-NOx-VOC limitation based on field data. *Atmospheric Environment*, **55**, 288–296, doi:10.1016/j.atmosenv.2012.03.061.

Chen, S., W. H. Brune, O. O. Oluwole, C. E. Kolb, F. Bacon, G. Li, and H. Rabitz, 2012: Global sensitivity analysis of the regional atmospheric chemical mechanism: an application of random

sampling-high dimensional model representation to urban oxidation chemistry. *Environmental science & technology*, **46 (20)**, 11 162–11 170, doi:10.1021/es301565w, PMID: 22963531.

Gao, D., W. R. Stockwell, and J. B. Milford, 1995: First-order sensitivity and uncertainty analysis for a regional-scale gas-phase chemical mechanism. *J. Geophys. Res.*, **100 (D11)**, 23 153–23 166, doi:10.1029/95JD02704, URL http://onlinelibrary.wiley.com/doi/10.1029/95JD02704/abstract.

Kleinman, L. I., P. H. Daum, Y.-N. Lee, L. J. Nunnermacker, S. R. Springston, J. Weinstein-Lloyd, and J. Rudolph, 2001: Sensitivity of ozone production rate to ozone precursors.

Morris, M. D., 1991: Factorial sampling plans for preliminary computational experiments. *Technometrics*, **33 (2)**, 161–174.

Sander, S., and Coauthors, 2011: Chemical Kinetics and Photochemical Data for Use in Atmospheric Studies, Evaluation No. 17. JPL Publication 10-6. URL http://jpldataeval.jpl.nasa.gov.

US EPA, 1999: Laboratory study to explore potential interferences to air quality monitors. Govt. Doc. EP 4.52:2002006990, Office of Air Quality Planning and Standards, Research Triangle Park, NC Accessed online: 2014-01-04.

Wilson, K. L., and J. W. Birks, 2006: Mechanism and elimination of a water vapor interference in the measurement of ozone by UV absorbance. *Environmental Science & Technology*, **40 (20)**, 6361–6367, PMID: 17120566.

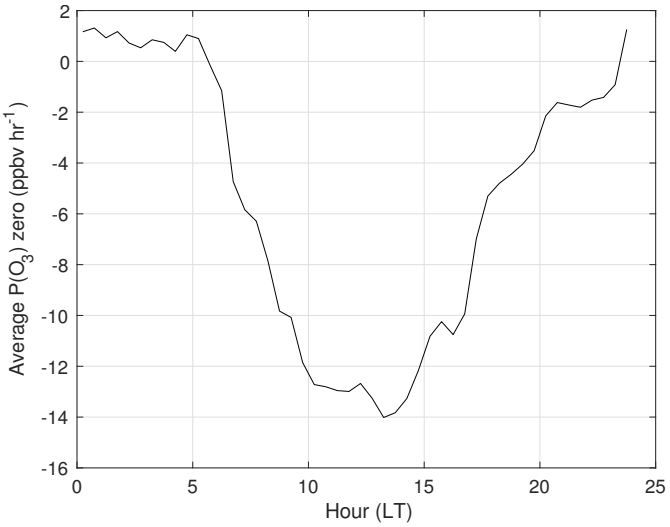


Figure S 1: Average zero correction for the MOPS raw $P(O_3)$ data. This diurnal zero is subtracted from the raw $P(O_3)$ data to derive the corrected $P(O_3)$ seen in the main text.

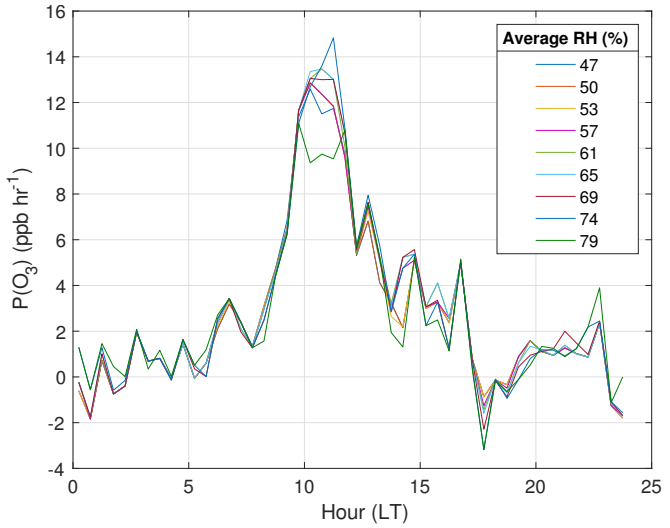


Figure S 2: Variation in the 24-hour corrected $P(O_3)$ by incrementally varying the MOPS analyzer temperature (and thus, relative humidity) filter. MOPS analyzer average relative humidities ranging from 50-80% for each temperature scenario from 21$^o$C (corresponding to 47% mean RH) to 12$^o$C. The MOPS corrected $P(O_3)$ shown is averaged for 30 minutes.

Table S 1: Median mixing ratios and standard deviations of all aircraft species measured in the vicinity of Golden, CO for MOPS measurement days. Constant, median values of these species supplement the canister VOC measurements in both MCMv331 and RACM2.

| VOC name | Mixing ratio (ppbv) | $\sigma$ (ppbv) |
|---|---|---|
| acetaldehyde | 1.32 | 0.72 |
| acetone | 3.51 | 1.02 |
| HCHO | 1.78 | 0.66 |
| nitric acid | 1.38 | 0.54 |
| MEK | 0.28 | 0.23 |
| methanol | 7.46 | 3.39 |
| MVK/methacrolein[a,b] | 100 | 50.8 |
| acetic acid | 0.40 | 0.38 |
| PAN[a] | 760 | 370 |
| PPN[a] | 110 | 60.0 |
| $H_2O_2$ | 1.90 | 0.77 |
| $CH_3OOH$ | 4.48 | 1.78 |
| HCOOH | 1.28 | 0.34 |
| ethanol | 1.00 | 1.09 |
| camphene[a] | 2.20 | 4.40 |
| d-limonene/3-carene[b] | 1.70 | 3.30 |

[a]In parts per trillion by volume (pptv)

[b]Methyl vinyl ketone and methacrolein are measured together; equal parts of each species is assumed in measurement. D-limonene/3-carene is grouped as limonene in MCMv331 and RACM2.

Table S 2: RACM2 RS-HDMR model input uncertainties adapted and estimated from Chen and Brune (2012) and modified for this study.

| Number | Model Input | Uncertainty ($1\sigma$,%) |
|---|---|---|
| 3 | *Meteorological parameters:* | $\leq 10$ |
| 7 | *Inorganics:* | |
| | Lowest: CO, $CO_2$ | 5 |
| | Highest: $O_3$,$NO_x$ | 10 |
| 32 | *VOC Groups:* | |
| | Lowest: ethene, ethane | 3 |
| | Highest: organic nitrates | >100 |
| | $JNO_2$ | 40[a] |
| 33 | TUV photolysis rates | 40[a] |
| 443 | *Reaction rate coefficients* | |
| | *Inorganic reactions:* | |
| | Lowest: OH + $H_2$ | 5[b] |
| | Highest: inorganics + $NO_3$, | 42[b,d] |
| | HONO + OH, NO + $O^3P$ | |
| | *Organic + OH:* | |
| | Lowest: ethane, ethanol, methanol | 10[b] |
| | Highest: ISO intermediate reactions | 75[a] |
| | *Organics + $NO_3$* | |
| | Lowest: $\alpha$-pinene | 15[d] |
| | Highest: DIEN (1,3-butadiene) | 133[d] |
| | *Organics + $O_3$* | |
| | Lowest: ISO | 19[c] |
| | Highest: isoprene nitrates, MOBA | 75[a] |
| | *Peroxy radical + NO* | 75[f] |
| | exceptions: ethene, $CH_3O_2$, | 144[b] |
| | TOL, unsaturated and aromatic aldehydes | |
| | and benzaldehyde | |
| | *$RO_2$ + $RO_2$ or $HO_2$* | 18-75[b,f] |
| | *PAN chemistry* | 18-27[b] |
| 615 | *Product yields* | 10-27[e] |

[a]Estimated
[b]NASA JPL (Sander et al., 2011)
[c]IUPAC
[d]Atkinson (1991)
[e]Gao et al. (1995) and references therein
[f]Estimated by Chen and Brune (2012)

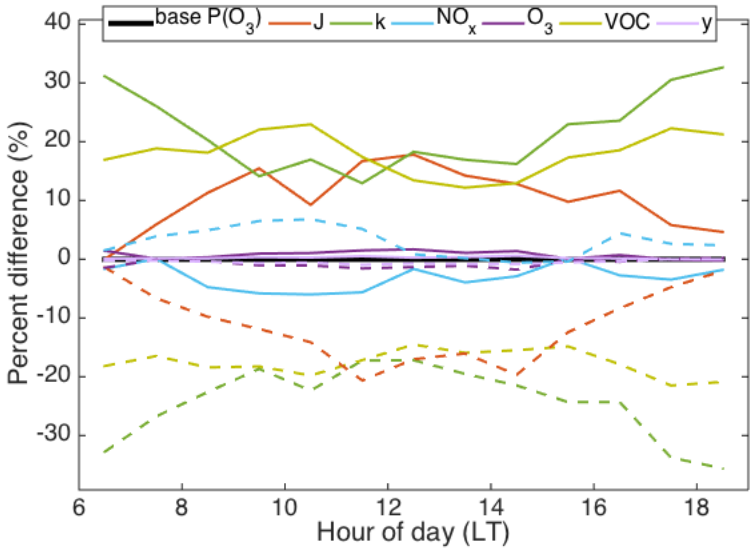


Figure S 3: MCM uncertainty analysis. Percent difference from base $P(O_3)$ calculated by increasing or decreasing the following parameters by their $1\sigma$ uncertainty levels: photolysis rates (J), select reaction rate coefficients (k), $NO_x = NO_2 + NO$, $O_3$, all measured VOCs, and select product yields (y). Solid (dashed) lines represent the percent difference from the base MCMv331 $P(O_3)$ run when each species is set to its upper (lower) limit.

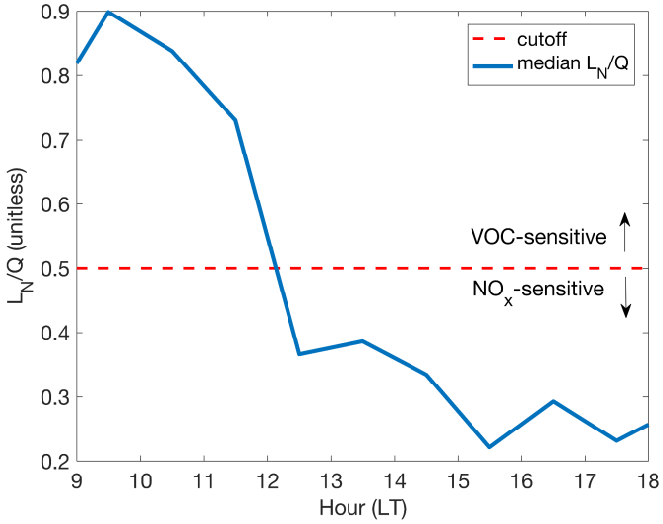


Figure S 4: Total median $L_N/Q$, representing the fraction of free radicals removed in the atmosphere by $NO_x$. $L_N/Q$ higher than 0.5 is considered to be within a VOC-sensitive regime, whereas $L_N/Q$ less than 0.5 is considered to be in a $NO_x$-sensitive regime.

Table S 3: Summary of select reaction rates and product yields varied for MCMv331 uncertainty analysis. Names of species are listed according to the RACM2 naming convention. Select reaction rates and product yields were varied all at once with all other constraints held at their original values.

| Rate coefficient | Uncertainty (%, $1\sigma$) | Product yield[e] | Uncertainty (%, $1\sigma$) |
|---|---|---|---|
| $k_{OH+NO_2}$ | 27[b] | Y(EPX + $O_3$ → $HO_2$) | 27 |
| $k_{HO_2+NO}$ | 14[b] | Y($CH_3OOH$ + OH → HCHO + OH ) | 18 |
| $k_{O^1D+H_2O}$ | 8[b] | Y(ISOP + NO → $HO_2$) | 27 |
| $k_{ACO_3+NO}$ | 42[b] | Y(HC3P + NO → $NO_2$) | 27 |
| $k_{PAN}$ | 18[b] | Y(XY2 → XYLP + HO2) | 27 |
| $k_{PPN}$ | 27[b] | Y(TR2 → products) | 27 |
| $k_{RCO_3+NO2}$ | 27[b] | | |
| $k_{OH+ACD}$ | 5[b] | | |
| $k_{RCO_3+NO}$ | 42[b] | | |
| $k_{EPX+O_3}$ | 75[a] | | |
| $k_{XYO+OH}$ | 14[d] | | |
| $k_{CH_3OOH+OH}$ | 40[b] | | |
| $k_{OH+HCHO}$ | 14[b] | | |
| $k_{XYM,XYP+OH}$ | 20[d] | | |
| $k_{ISO+OH}$ | 10[c] | | |
| $k_{ETE+OH}$ | 18[b] | | |
| $k_{ACO_3+NO_2}$ | 18[b] | | |

[a]Chen and Brune (2012)
[b]NASA JPL (Sander et al., 2011)
[c]Atkinson et al. (2006)
[d]Atkinson and Aschmann (1989)
[e]Gao et al. (1995)

Table S 4: Golden, CO RACM2 and MCMv331 model relative uncertainties ($1\sigma$) between 0600 and 1800 local time.

| **Time of day (LT)** | 0600-0800 | 0800-1000 | 1000-1200 | 1200-1400 | 1400-1800 |
|---|---|---|---|---|---|
| RACM2 Uncertainty (%) | 30 | 33 | 31 | 28 | 28 |
| MCMv331 Uncertainty (%) | 33 | 30 | 30 | 28 | 32 |